Modeling of Ni Diffusion Induced Austenite Formation in Ferritic Stainless Steel Interconnects

Chen, Ming; Alimadadi, Hossein; Molin, Sebastian; Zhang, L.; Ta, Na; Hendriksen, Peter Vang; Kiebach, Wolff-Ragnar; Du, Y.

Published in:
Electrochemical Society. Journal

Link to article, DOI:
10.1149/2.1711709jes

Publication date:
2017

Document Version
Peer reviewed version

Modeling of Ni Diffusion Induced Austenite Formation in Ferritic Stainless Steel Interconnects [**]

M. Chen [a, *], H. Alimadadi[b], S. Molin[a], L. Zhang[c], N. Ta[a,c], P. V. Hendriksen[a], R. Kiebach[a], and Y. Du[c]

[a] Department of Energy Conversion and Storage, Technical University of Denmark, Roskilde 4000, Denmark

[b] Center for Electron Nanoscopy, Technical University of Denmark, Lyngby 2800, Denmark

[c] State Key Laboratory of Powder Metallurgy, Innovative Materials Design Group, Central South University, Changsha, Hunan 410083, China

[*] Corresponding author. Tel.: +45 46775757; Fax: +45 46775858; Email: minc@dtu.dk.

[**] Part of this manuscript has been published previously in *ECS Transactions* (M. Chen, S. Molin, L. Zhang, N. Ta, P. V. Hendriksen, W. R. Kiebach, and Y. Du, "Modeling of Ni Diffusion Induced Austenite Formation in Ferritic Stainless Steel Interconnects", *ECS Transactions,* **68** [1] 1691-1700 (2015).).

Abstract

Ferritic stainless steel interconnect plates are widely used in planar solid oxide fuel cell and electrolysis cell stacks. During stack production and operation, nickel from the Ni/yttria stabilized zirconia fuel electrode or from the Ni contact component layer diffuses into the interconnect plate, causing transformation of the ferritic phase into an austenitic phase in the interface region. This is accompanied with changes in volume, and in mechanical and corrosion properties of the interconnect plates. In this work, kinetic modeling of the inter-diffusion between Ni and FeCr based ferritic stainless steel was conducted, using the CALPHAD (CALculation of PHAse Diagrams) approach with the DICTRA (DIffusion Controlled TRAnsformation) software. The kinetics of inter-diffusion and austenite formation was explored in detail. The simulation was further validated by comparing with experiments. The results show that after 2000 h at 800 ^{o}C Ni diffuses more than 100 μm deep into Crofer 22 APU. Along with the Ni diffusion, part of the ferritic steel with 50-60 μm in thickness has transformed into the austenitic phase. Growth of the austenite phase in commercial interconnect materials was predicted to take place under practical stack operation conditions.

Introduction

Owing to their high temperature stability and relatively low cost, chromia-forming ferritic stainless steels are widely used as interconnect materials in solid oxide fuel cell (SOFC) and electrolysis cell (SOEC) stacks. This type of steel typically has a chromium content of 20 - 30 wt.%. The thermal expansion coefficient (TEC) matches well with that of anode supported solid oxide cells (SOCs) [1]. During high temperature oxidation, a chromium oxide scale forms on the steel, which has a reasonable electronic conductivity at typical SOFC/SOEC operating temperature (650 – 850 ^{o}C) [2]. For practical applications, protective coatings are required especially for the oxygen side, to enhance the oxidation resistance and the electrical conductivity of the formed oxide scale and to mitigate Cr evaporation. Recent progress on alloy and coating development for ferritic stainless steel interconnects has been reviewed by Shaigan et al. [3].

In the so-called planar stack design, a certain number of planar SOCs are stacked, with shaped interconnects (ICs) in between. These plates serve as interconnects and separate the neighboring fuel and oxygen electrode compartments of adjacent cells. An intimate contact between the electrodes and the IC plate is essential to ensure optimum cell and stack performance. During stack production and operation, inter-diffusion of elements across the cell – IC interface takes place, which under certain circumstances introduces adverse effects on the electrical, mechanical, and corrosion properties of the IC plates, and may further damage the electrodes. One representative example is the diffusion of nickel from the Ni/YSZ fuel electrode or from the Ni contact component layer into the IC plate, while iron and chromium from the steel diffuse in the opposite

direction. Diffusion of Ni into the steel causes transformation of the ferritic (BCC) phase into the austenitic (FCC) phase in the interface region, accompanied with changes in volume and in mechanical and corrosion properties of the IC plates. A number of studies have been devoted to investigate this process experimentally. Sakai et al. reported a radial pattern of Ni diffusion into ZMG232 [4]. Chromium depletion and internal oxidation occurred in the diffusion zone. Pre-oxidation of the steel was reported to be effective in suppressing the inter-diffusion, but resulted in an increase of the contact resistance. Quadakkers and his co-workers investigated Ni diffusion and formation of the austenite phase in both long-term tested SOFC stacks and model samples including a Ni mesh in contact with Crofer 22 APU or Crofer 22 H [2, 5]. In addition to austenite, formation of sigma (σ) phase was detected in the interface region [2]. The experiments were correlated to the thermodynamics of the Fe-Cr-Ni system. Authors of the current work have previously reported reduced oxidation kinetics in Ni electroplated Crofer 22 APU as compared to uncoated ones [6]. This was attributed to slow diffusion kinetics of the FCC phase (2 - 3 orders of magnitude slower than in BCC). Recently, Harthøj et al. studied Ni diffusion from the Ni/YSZ fuel electrode into Crofer 22 APU and its influence on the contact resistance across the interface [7]. It was concluded that the inter-diffusion introduces microstructural instability, but also lower electrical resistance (due to formation of metallic pathways). Similar studies have also been conducted by Mikkelsen et al. [8], who investigated long-term oxidation behavior and electrical interface resistance between FeCr alloy sheets and Ni/YSZ plates. Their results show that metallic bridges exist through the formed oxide scale even after 1 year of operation.

In this work, kinetic modeling of the inter-diffusion between Ni and FeCr based ferritic stainless steel was conducted, using the CALPHAD (CALculation of PHAse Diagrams) approach with the DICTRA (DIffusion Controlled TRAnsformation) software. To give a full account of the observed experimental phenomena, the following processes have to be taken into account: (i) inter-diffusion and transformation of ferrite into austenite, (ii) oxide scale formation, and (iii) formation of σ phase. The present work focuses on the first process only. Here kinetic modeling of inter-diffusion and austenite formation was explored in detail, as functions of temperature and time plus influence of grain boundary diffusion. The simulation was further validated by comparing with experimental results.

Experimental and Kinetic Modeling

We have previously reported on the oxidation kinetics of Ni coated Crofer 22 APU (ThyssenKrupp VDM, Germany) in humidified H_2/N_2 [6]. The samples consisted of 300 μm thick Crofer 22 APU flat sheets electroplated with pure Ni on both sides. Crofer 22 APU contains typically 20-24 wt.% Cr, 0.3-0.8 wt.% Mn with some minor elements (La, Ti) and Fe as a balance. For an exhaustive list of the chemical composition, the readers are referred to our previous study [1]. The oxidation study was carried out at 800 ^{o}C in a mixture of 4 % H_2O + 9 % H_2 + 87 % N_2 for periods up to 2000 hours. Detail on the oxidation kinetics and microstructural evolution is presented elsewhere [6]. The microstructure of one specific sample, namely the 13 μm thick Ni coated Crofer 22 APU oxidized for 2000 h, was further investigated in the present work and the post-test results were employed to validate the modeling results. Polished cross-sections were first

examined using a Supra 35 scanning electron microscope equipped with a field emission gun (FE-SEM, Carl Zeiss). Chemical compositions were obtained via an X-ray Energy Dispersive Spectrometer (EDS) with data analysis using a microanalysis software NSS (Thermo Fischer Scientific Inc.). In addition, backscatter electron imaging was carried out in a FEI Helios NanoLab^{TM} 600 dual beam microscope equipped with a field-emission gun using accelerating voltage of 20 kV and probe current of 1.4 nA. For phase differentiation, electron backscatter diffraction (EBSD) was performed in a FEI Nova NANOSEM 600 equipped with a field-emission gun. The FEI Nova NANOSEM 600 was also equipped with an EBSD system from Bruker, e^{-}Flash^{HR} camera, and an ARGUS electron imaging system (all Bruker Nano GmbH, Berlin, Germany). The EBSD measurement was performed in a square grid with an electron probe current of 3.1 nA at an acceleration voltage of 20 kV, and camera exposure time of 7 ms. EBSD data analysis was carried out using Esprit 2.0.

The modeling part was carried out using the CALPHAD approach with the Thermo-Calc and DICTRA software [9]. Thermo-Calc is a powerful tool for phase equilibrium, phase diagram and phase transformation calculations, whereas DICTRA is a software package for simulation of diffusional reactions in multicomponent alloys. For further detail on Thermo-Calc and DICTRA, the readers are referred to the paper by Andersson et al. [9] and Borgenstam et al. [10]. In this work, the thermodynamics and phase relations of relevant systems were explored using Thermo-Calc and TCFE7 database. For kinetic modeling, a 1D diffusion couple was set up (shown in Figure 1), where metallic Ni coating (FCC, denoted by Phase γ in the current work) is in contact with FeCr-based ferritic stainless steel (BCC, Phase α). The inter-diffusion across the interface and the

transformation of ferrite into austenite was modelled using DICTRA in conjunction with both TCFE7 and MOBFE2 databases.

Results and Discussion

Model Experiment of Ni Diffusion into Crofer 22 APU

Figure 2a presents a backscatter electron (BSE) image on the polished cross-section of 13 μm Ni coated Crofer 22 APU after 2000 h oxidation at 800 ^{o}C. The contrast in the micrograph stems from the difference in chemical compositions and crystallographic orientation. As reported previously [6], the Ni coating remains metallic after electroplating. After 2000 h oxidation, most of the Ni has diffused into the steel. A small number of Ni particles remains on the surface of the formed oxide scale. The oxide scale has a thickness of about 2 μm and has some metallic particles (Ni/Fe rich) as inclusions. At about 60-70 μm from the oxide scale an abrupt change in contrast can be easily seen in Figure 2a indicating either crystallographic orientation and/or chemical compositional change. The EDS elemental mapping of the scanned area is shown in Figure 2b. The oxide scale consists of mainly Cr and Mn, corresponding most likely to an outer layer of $(Cr,Mn)_3O_4$ spinel and an inner layer of Cr_2O_3, as reported previously [6]. In the bulk of the steel, the contrast difference observed in Figure 2a is reflected as change of Cr/Ni/Fe concentrations as shown in Figure 2b. No secondary phase (e.g. σ phase) seems to appear in the examined area.

Based on the obtained area spectra imaging data, an integrated EDS line-scan was made. The line was drawn perpendicular to the oxide scale – steel interface. Data over the entire area were then integrated along the line. Figure 2c plots the atomic percentages of Fe, Cr, Ni, Mn from the oxide scale – steel interface into the steel, while the other elements are excluded. As expected, significant inter-diffusion took place after 2000 h at 800 ^{o}C. The Ni content is above 1.5 at.% at a distance of ~95 μm from the oxide scale – steel interface, indicating Ni diffuses deeper than the area investigated in the EDS measurement. There seems to be a relatively sharp increase in the Cr content and a decrease in the Ni content at the distance of 65 μm, in accordance with the contrast change shown in Figure 2a.

The sample was further examined using FEI Helios NanoLab^{TM}600 and FEI Nova NANOSEM 600 to obtain information on the phases and microstructure of different layers. As shown in Figure 3a, starting just beneath the oxide scale to the bulk of the steel, 4 distinct layers with different grain structure and orientations are clearly visible. The layer just beneath the oxide scale (hereafter named as Layer 1) has a thickness of ~10 μm and a grain size of 3 – 5 μm. Layer 2 has a thickness of around 25-35 μm and consists of much bigger grains, with a grain size of 8 – 10 μm. Layer 3 has a thickness of about 30 μm and the finest grain structure among all the 4 layers. Layer 4, located at the bottom of Figure 3a, has much coarser grains, pancake-like which are elongated parallel to the steel sheet. The grains are 60-80 μm in width and 300-400 μm in length. By comparing Figure 3a with Figure 2, it becomes evident that the boundary between Layer 3 and Layer 4 corresponds to the contrast change shown in Figure 2a and the sharp change of Cr/Ni content in Figure 2c. Besides, it is worth noting that the boundaries between the oxide

scale and Layer 1 and between Layer 1 and layer 2 are quite parallel to the sample surface, while the ones between Layer 2 and layer 3 and between Layer 3 and Layer 4 are a bit wavy.

Figure 4a shows the electron backscatter pattern quality (EBSP-Q) map of an area measured by EBSD. EBSP-Q maps have been extensively used for revealing grain boundaries and local strain in various steels [11]. There is strong resemblance between Figure 4a and Figure 3a, indicating that the area investigated by EBSD is representative of the material system and all four layers are covered. In Figure 4b the phase color-coded map (ferrite: green and austenite: red) is overlaid on the EBSP-Q map (Figure 4a). It is evident that the majority of grains in Layers 1 and 2 are indexed as FCC austenite while those in Layers 3 and 4 are mainly indexed as BCC ferrite. Even though Layer 3 is mainly indexed as BCC ferrite, the microstructure features resemble those of martensite [12]. Martensite has a crystal structure of body centered tetragonal (BCT), and the tetragonality (c/a ratio) is dependent on the carbon content [13]. Since c/a ratio is for most cases close to unity, EBSD cannot differentiate between BCC ferrite and BCT martensite.

As discussed earlier, the abrupt change in Cr/Ni content happens at the boundary between Layer 3 and Layer 4, while the chemical compositions of Layers 2 and 3 are comparable. Additionally, martensite forms as a result of solid state phase transformation of austenite upon cooling. Hence, Layer 3 must have formed as the sample was cooling down from 800˚C. Reconstructing the pre-austenite grains from EBSD data can be done assuming specific orientation relations between the austenite and martensite [14].

However, using backscatter electron images it is also possible, though subjectively [7], to reconstruct the pre-austenite grains. Color orientation contrast imaging using backscatter electrons [15] are especially helpful for pre-austenite grain boundary reconstruction, as shown in Figure 5. The reconstructed pre-austenite grains of Layer 3 (Figure 5b) show that the grain sizes of the two mentioned layers (2 and 3) are comparable. Hence, one can conclude that Layers 2 and 3 at elevated temperature are actually of the same phase (austenite) but with different chemical compositions (see Figure 2). However, upon cooling down to room temperature Layer 3 forms due to a martensitic phase transformation whereas Layer 2 remains austenitic. One may see this as a discrepancy, but there are two differences between layers 2 and 3 which influence the thermodynamics and kinetics of solid state phase transformation: (i) Layer 2 has higher nickel content and Ni is a well-known austenite stabilizer (see the discussion of Phase diagrams below). (ii) There is a very large interface between the Layer 3 and Layer 4 (BCC ferrite). The BCC ferrite is an excellent site for martensite nucleation based on the martensite heterogeneous nucleation mechanism [16]. There is an autocatalytic behavior associated with the martensitic phase transformation, i.e. upon nucleation and formation of martensite, new sites for nucleation develop [16]. Thus, Layers 2 and 3 which seemingly cannot be distinguished at elevated temperature are differentiated at room temperature by the difference in thermodynamics and kinetics of phase transformation to martensite.

Phase Diagrams of Fe-Cr-Ni

As shown in Figure 2, a thin layer of oxide scale formed on each side of the Ni coated steel sample. As compared to the 300 μm thick steel, the oxide scale has a thickness of

only 4 μm (i.e. 2 μm on both sides) and is therefore expected to have a minor influence on the steel bulk composition. If the oxide scale were formed in advance, it would act as a diffusion barrier layer between Ni and the steel. Considering the fact that in the current study most of the coated Ni has diffused into the steel, the formation of the continuous oxide scale should then occur after transformation of the original Ni coating into a NiFeCr austenite solid solution (i.e. Layer 1 in Figure 3). As the oxide layer forms on top of Layer 1, it should have minor influence on the interdiffusion process between Ni and FeCr steel, i.e. the interdiffusion process taking place inside Layers 1-4. Formation of oxide scale may however have an influence on the local chemistry at the oxide scale – Ni/Steel interface. This will be considered in future work, when all the 3 processes (inter-diffusion and formation of austenite, oxidation, and formation of σ phase) will be modelled together. In the present work, the inter-diffusion and transformation of ferrite into austenite across the Ni – Steel interface is modelled. Figure 6 presents the phase diagram of Fe-Cr-Ni calculated at two different temperatures. At 800 ^{o}C, the α phase has rather limited Ni solubility, while the γ phase, originating from pure Ni, has a wide solubility range for both Fe and Cr. The single-phase region of σ starts from the Fe-Cr binary and extends into the ternary, towards the Cr-rich corner. At 900 ^{o}C, the σ single-phase region exists only in the ternary system. The 700 ^{o}C phase diagram (not shown here) is similar to the one at 800 ^{o}C, except that the solubility of Ni in the α phase is slightly higher.

Modeling of Ni Diffusion into $Fe_{0.76}Cr_{0.24}$ (Bulk Diffusion only)

As shown in Figure 1, a diffusion couple of Ni – Steel was set up which mimics the experiments. As the experimental sample (Crofer 22 APU metal sheet, 300 μm in thickness) was coated with Ni on both sides, due to the existing symmetry only half of the sample was modelled. Crofer 22 APU has about 20 – 24 wt.% Cr, 0.3 – 0.8 wt.% Mn plus some minor elements (La, Ti, etc.) and Fe as a balance [1, 2, 6]. In the current work, modeling was carried out on a diffusion couple of 13 μm Ni – 150 μm $Fe_{0.76}Cr_{0.24}$ (i.e. Fe/Cr = 76/24 in atomic ratio and 77/23 in mass ratio). At first, only bulk diffusion is considered. The composition profiles along the diffusion couple at different time steps are presented in Figure 7 for the time periods up to 2000 h at 800 ^{o}C. As expected, Ni diffuses into the steel while Fe and Cr diffuse in the opposite direction. In agreement with the thermodynamics (Figure 6), the content of Ni in the α phase (the right part of diffusion couple) is rather low all the way from the interface to the right boundary, while the contents of Fe and Cr in the γ phase decrease continuously with the distance from the interface.

Based on the composition profiles, the Ni diffusion distance can then be evaluated as the distance from the original γ/α interface at *Time* = 0 h (i.e. Distance = 13 μm in Figure 1) to the point where the Ni content in the γ phase reaches below 0.5 wt.%. The results are plotted in Figure 8a for 700, 800, and 900 ^{o}C. At 800 ^{o}C, a Ni diffusion distance of 71.6 μm is obtained from DICTRA modeling, where only bulk diffusion is considered. Accompanied with inter-diffusion, the γ/α interface moves towards right. Figure 8b shows the thickness of the γ layer as a function of time at 700 – 900 ^{o}C. At 800 ^{o}C, the γ layer thickness increased from 13 μm at *Time* = 0 h (i.e. the Ni coating thickness) to 19 μm at *Time* = 2000 h. According to the experimental results, the Ni diffusion distance in

Crofer 22 APU is beyond 100 μm for 2000 h diffusion at 800 ^{o}C. As shown in Figure 8b, the experimentally measured γ layer thickness is about 60-70 μm (i.e. the distance from the oxide scale/metal interface to the boundary between Layer 3 and Layer 4 in Figure 3), much thicker than the value predicted from the simulation. DICTRA modeling seems to under-estimate the inter-diffusion and hence also the accompanied $\alpha \rightarrow \gamma$ phase transformation, when only bulk diffusion is considered.

Figure 9 plots the intrinsic diffusion coefficients of Cr, Ni and Fe in the α (BCC) and γ (FCC) phases along the diffusion couple length at *Time* = 2000 h. There is an obvious difference in the component diffusion rates in the two phases. All of the components diffuse much faster in the α phase than in γ. The difference is about two orders of magnitude. Fe appears to be the fatest diffusion component in the α phase, followed by Cr and Ni. In the γ phase, the difference in the diffusion rates of the three elements is relatively smaller and Cr appears to be the fastest one. Transformation of α into γ significantly slows down the Cr/Fe outward diffusion. This explains well the reduced oxidation kinetics in Ni electroplated Crofer 22 APU as compared to uncoated ones [6]. It can be futher concluded that the Ni inward diffusion (especially the one in the γ phase) is the rate-limiting step for the α - γ transformation.

Modeling of Ni Diffusion into $Fe_{0.76}Cr_{0.24}$ (Bulk + Grain Boundary Diffusion)

To properly account the experimental data, grain boundary diffusion should also be considered. Grain boundary diffusion is important and often non-negligible contributor to

the total diffusion, especially at low temperatures. The grain boundary diffusion model in DICTRA was next employed [10] to the case at hand. The grain boundary diffusion is correlated to the bulk diffusion by using the same frequency factor, but a modified bulk activation energy, as specified by the equation below:

$$M^{gb} = M_0^{bulk} \cdot \exp(F_{redGB} \cdot Q^{bulk}/R/T) \qquad [1]$$

where M^{gb} is the mobility in the grain boundary, M_0^{bulk} and Q^{bulk} are the frequency-factor and activation energy in the bulk, respectively, and F_{redGB} is the bulk diffusion activation energy multiplier. The total mobility including both bulk and grain boundary diffusion is then formulated as:

$$M^{Total} = \delta/d \cdot M^{gb} + (1- \delta/d) \cdot M^{bulk} \qquad [2]$$

where δ, d, and M^{bulk} are the grain boundary thickness, the grain size as a function of time and temperature, and the mobility in the bulk, respectively. The grain boundary diffusion model in DICTRA requires three input parameters: F_{redGB}, δ and d. In the current work, grain boundary diffusion is considered for both the α and γ phases. Here the grain size was assumed to be constant with time, which reduces the complexity of system without sacrificing the accuracy of predictions of the model. A grain size of 50 and 5 μm was adopted for the α and γ phases, respectively, according to the results reported by Garcia-Fresnillo et al. [2]. This is also in qualitative agreement with the grain size shown in Figure 3, even though there the sample has been heat treated at 800 ^{o}C for 2000 h. The grain size of electroplated Ni is in submicron range, and after 30 minutes at

elevated temperature the grain growth changes minimally with temperature [17]. Hence, when long time treatment is considered, the grain growth of Ni at the very early stage can be neglected. The grain boundary thickness δ was set as $0.5 \cdot 10^{-10}$ m, as recommended by DICTRA. The bulk diffusion activation energy multiplier F_{redGB} was varied between 0.5 and 0.7. The best fit to the experimental data (shown in Figure 10a) was achieved at $F_{redGB} = 0.65$ for both α and γ phases. Figure 10a presents the simulated composition profile in comparison with the experimental results obtained from the present work (Figures 2-4). As shown in Figures 2-4, after 2000 h at 800 ^{o}C, most of the Ni has diffused into the steel and the original Ni – steel interface is replaced by the oxide scale – steel interface. This point was then set as "distance zero" as for the experimental data points. As shown in Figure 10a, with the chosen parameters, the DICTRA modeling results are in reasonable agreement with the experimental ones. The γ phase layer has grown to 63 μm in thickness (including the initial 13 μm Ni coating). By plotting the composition profile onto the ternary phase diagram, the diffusion path at different time steps can be illustrated. This is shown in Figure 10b. Four time steps are included: 1 h, 100 h, 1000 h, and 2000 h. At time = 1 h, the diffusion path starts from pure Ni and travels through the γ single-phase region all the way to the $\alpha+\gamma$ two-phase region and ends at the composition $Fe_{0.76}Cr_{0.24}$. The change to the diffusion path with time happens mainly in the γ single-phase region, which is due to its wide composition range and slower diffusion kinetics (two orders of magnitude slower than that of the α phase). The diffusion path in the $\alpha+\gamma$ two-phase region moves slowly towards the $\alpha+\gamma+\sigma$ three-phase triangle. Thermodynamic calculations suggest that the equilibrium state of the given system (13 μm thick Ni + 150 μm thick $Fe_{0.76}Cr_{0.24}$) is a $\gamma+\sigma$ two-phase mixture. Continuing after 2000 h, the diffusion path will travel through the $\alpha+\gamma+\sigma$ three-phase

triangle and end in the γ+σ two-phase region eventually. To successfully model the entire process, diffusion in multi-phase mixtures should be properly accounted for. This will be presented in the future.

Figure 11 plots the predicted thickness of the γ layer in the diffusion couple of Ni – $Fe_{0.76}Cr_{0.24}$ heat treated at 800 ^{o}C for periods up to 2000 h. For comparison, the experimentally measured values are also included. These values were obtained by measuring the thickness of the three layers (Layers 1+2+3 in Figure 3a) from the SEM backscatter images at 20-30 different locations. As mentioned before, the boundary between Layer 3 and Layer 4 is quite wavy, which gives a quite large scatter in the experimentally measured γ layer thickness. But still, the DICTRA simulations agree reasonably well with the experimental values, also for the sample heat treated for only 1000 h, where the experimental results were not taken into account when adjusting parameters for the grain boundary diffusion.

Conclusions

In the current work, the inter-diffusion between Ni and ferritic steel interconnects was investigated by means of both experiments and theoretical diffusion modeling employing the DICTRA software in conjunction with both thermodynamic and diffusion databases. The experimental results show that after 2000 h at 800 ^{o}C Ni diffuses more than 100 μm deep into the Crofer 22 APU steel. Along with the Ni diffusion, part of the ferritic steel with 50-60 μm in thickness has transformed into the austenitic phase. DICTRA modeling gives a proper account of the experimental results on inter-diffusion and accompanied α

374 $\rightarrow \gamma$ phase transformation, when both bulk and grain boundary diffusion are considered.
375 The Cr diffusion rate is significantly reduced with the α-to-γ phase transformation,
376 accounting well for the reduced oxidation kinetics of Ni electroplated samples. The
377 simulation identifies also the rate limiting step of the α-to-γ phase transformation, being
378 the Ni inward diffusion, especially in the γ phase. The present work provides a proper
379 account of the thermodynamics and kinetics of Ni-steel inter-diffusion and the results
380 could be employed to further analysis of associated changes in the mechanical and
381 corrosion properties of the IC plates, which will be presented near future.
382
383 **Acknowledgments**
384
385 The projects ForskEL 2013-1-12013 “Solid Oxide Electrolysis for Grid Balancing”
386 funded by Energinet.dk and EUDP 64012-0225 “SOFC Accelerated – Development to
387 Accelerate Field Demonstrations” funded by Danish Energy Agency are gratefully
388 acknowledged. The A.P. Møller and Chastine Mc-Kinney Møller Foundation is gratefully
389 acknowledged for their contribution toward the establishment of the Center for Electron
390 Nanoscopy at the Technical University of Denmark.
391
392 **References**
393 1. M. Palcut, L. Mikkelsen, K. Neufeld, M. Chen, R. Knibbe, and P. V. Hendriksen,
394 *Corros. Sci.*, **52**, 3309 (2010).
395 2. L. Garcia-Fresnillo, V. Shemet, A. Chyrkin, L. G. J. de Haart, and W. J. Quadakkers,
396 *J. Power Sources*, **271**, 213 (2014).
397 3. N. Shaigan, W. Qu, D. G. Ivey, and W. Chen, *J. Power Scources*, **195**, 1529 (2010).

4. N. Sakai, T. Horita, K. Yamaji, Y. P. Xiong, H. Kishimoto, M. E. Brito, and H. Yokokawa, *Solid State Ionics*, **177**, 1933 (2006).

5. J. Froitzheim, L. Niewolak, M. Brandner, L. Singheiser, and W. J. Quadakkers, *J. Fuel Cell Sci. Technol.*, **7**, (2010).

6. S. Molin, M. Chen, J. R. Bowen, and P. V. Hendriksen, *ECS Trans.*, **57**, 2245 (2013).

7. A. Harthoj, H. Alimadadi, T. Holt, and P. Moller, *J. Electrochem. Soc.*, **162**, F387 (2015).

8. L. Mikkelsen, J. Hogh, and P. V. Hendriksen, in *Proceeding of the 8th European SOFC Forum*, p. A0905, Lucerne, Switzerland (2008).

9. J.-O. Andersson, T. Helander, L. Hoglund, P. Shi, and B. Sundman, *CALPHAD*, **26**, 273 (2002).

10. A. Borgenstam, L. Hoglund, J. Agren, and A. Engstrom, *J. Phase Equilib.*, **21**, 269 (2000).

11. S. I. Wright and M. M. Nowell, *Microsc. Microanal.*, **12**, 72 (2006).

12. S. Morito, H. Tanaka, R. Konishi, T. Furuhara, and T. Maki, *Acta Mater.*, **51**, 1789 (2003).

13. L. Ryde, *Mater. Sci. Technol.*, **22**, 1297 (2006).

14. C. Cayron, *J. Appl. Crystallogr.*, **40**, 1183 (2007).

15. A. P. DAY and T. E. QUESTED, *J. Microscopy*, **195**, 186 (1999).

16. G. B. Olson and Z. D. Feinberg, in *Woodhead Publishing Series in Metals and Surface Engineering*, p. 59, Woodhead Publishing, (2012).

17. A. J. Detor and C. A. Schuh, *J. Mater. Res.*, **22**, 3233 (2007).

Figure Captions

Figure 1. Schematic illustration of the diffusion couple between Ni coating (left) and FeCr-based ferritic stainless steel used for IC (right).

Figure 2. (a) Backscatter electron image and (b) EDS elemental map on the polished cross-section of the oxide scale – steel (Crofer 22 APU) interface; (c) Integrated EDS line-scan perpendicular to the oxide scale – steel (Crofer 22 APU) interface. The sample is a 300 μm thick Crofer 22 APU sheet coated with 13 μm thick Ni coating on both sides, further heat treated at 800 ^{o}C in H_2+N_2+H_2O for 2000 h.

Figure 3. (a) Backscatter electron image covering all four distinct layers in the steel. (b) A higher magnification backscatter electron image of the region marked by the black square in (a) showing the fine-grained microstructure of Layer 3.

Figure 4. (a) Electron backscatter pattern quality (EBSP-Q) map of an area covering all four layers. (b) Color coded phase map (ferrite: green and austenite: red) overplayed on EBSP-Q map.

Figure 5. (a) ARGUS^{TM} image [15] of the Layers 2, 3 and 4. (b) A subjective reconstruction of pre-austenite grains of Layer 2 and Layer 3.

Figure 6. Phase diagrams of Fe-Cr-Ni at 800 and 900 ^{o}C. In the diagrams all the single-phase regions have been marked: α - BCC (ferrite), γ - FCC (austenite), and σ. The red

443 triangles indicate 3-phase equilibrium ($\alpha+\gamma+\sigma$), while the remaining unmarked regions
444 are 2-phase equilibria ($\alpha+\gamma$, $\gamma+\sigma$, or $\alpha+\sigma$).
445
446 Figure 7. Calculated composition profiles (in mole fraction) along the diffusion couple of
447 Ni – $Fe_{0.76}Cr_{0.24}$ heat treated at 800 ^{o}C for periods up to 2000 h. The initial thickness was
448 13 μm and 150 μm for the Ni and $Fe_{0.76}Cr_{0.24}$ layers, respectively. Only bulk diffusion
449 was considered here.
450
451 Figure 8. (a) Calculated Ni diffusion distance and (b) thickness of the γ layer in the
452 diffusion couple of Ni – $Fe_{0.76}Cr_{0.24}$ heat treated at 700-900 ^{o}C for periods up to 2000 h.
453 The initial thickness was 13 μm and 150 μm for the Ni and $Fe_{0.76}Cr_{0.24}$ layers,
454 respectively. The Ni diffusion distance is defined as the distance from the initial γ/α
455 interface at 0 h (i.e. Distance = 13 μm in Figure 1) to the position where the Ni content
456 reaches below 0.5 wt.%. Only bulk diffusion was considered here.
457
458 Figure 9. Intrinsic diffusion coefficients of Cr, Ni and Fe in α and γ phases along the
459 diffusion couple of Ni – $Fe_{0.76}Cr_{0.24}$ heat treated at 800 ^{o}C at *Time* = 2000 h. Only bulk
460 diffusion was considered here.
461
462 Figure 10. (a) Left: Simulated composition profiles (in mole fraction) along the diffusion
463 couple of Ni – $Fe_{0.76}Cr_{0.24}$ heat treated at 800 ^{o}C for periods up to 2000 h. The initial
464 thickness was 13 μm and 150 μm for the Ni and $Fe_{0.76}Cr_{0.24}$ layers, respectively. Both
465 bulk and grain boundary diffusion are considered. The experimental data points are from
466 the present work (Figure 2c). Mn was excluded in calculating mole fraction; (b) Right:

diffusion path at 1 h (red), 100 h (green), 1000 h (blue), 2000 h (pink) super-imposed onto the Fe-Cr-Ni phase diagram at 800 ^{o}C.

Figure 11. Thickness of the γ layer in the diffusion couple of Ni – $Fe_{0.76}Cr_{0.24}$ heat treated at 800 ^{o}C for periods up to 2000 h. The initial thickness was 13 μm and 150 μm for the Ni and $Fe_{0.76}Cr_{0.24}$ layers, respectively. The experimental values were obtained from SEM image analysis, where the thickness of Layers 1+2+3 was measured at 20-30 different locations.

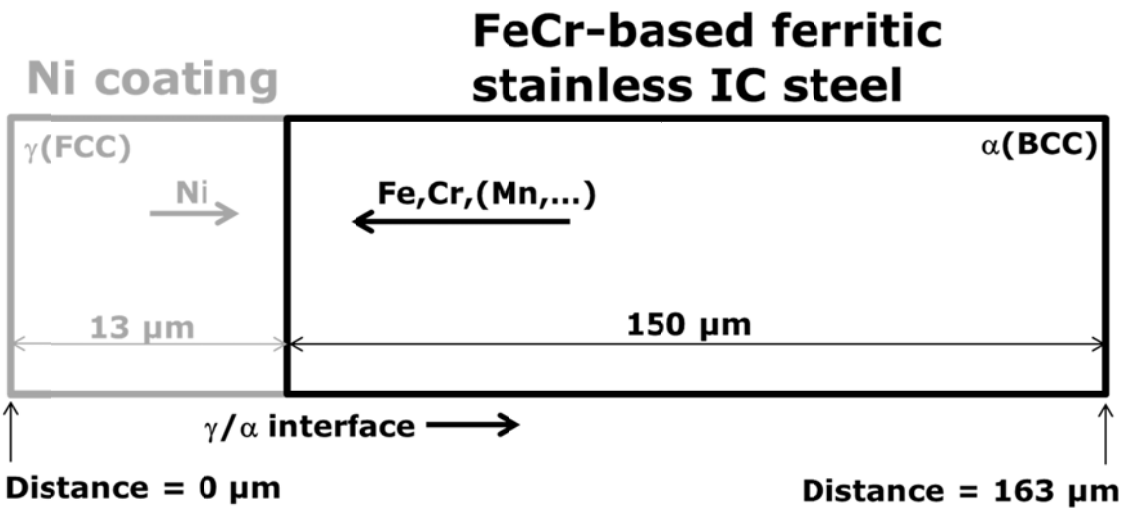

481

483 Figure 1. Schematic illustration of the diffusion couple between Ni coating (left) and

484 FeCr-based ferritic stainless steel used for IC (right).

484

485

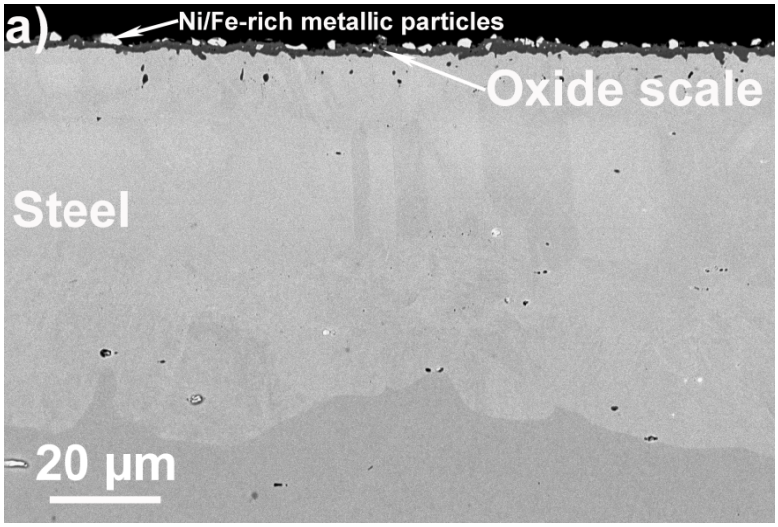

486

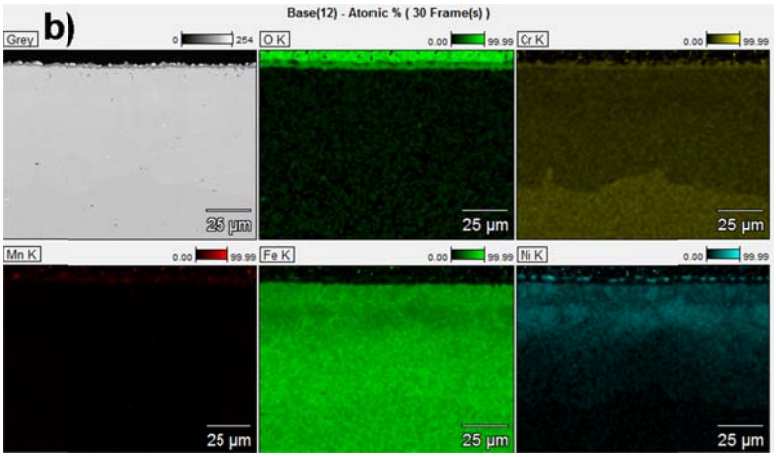

487

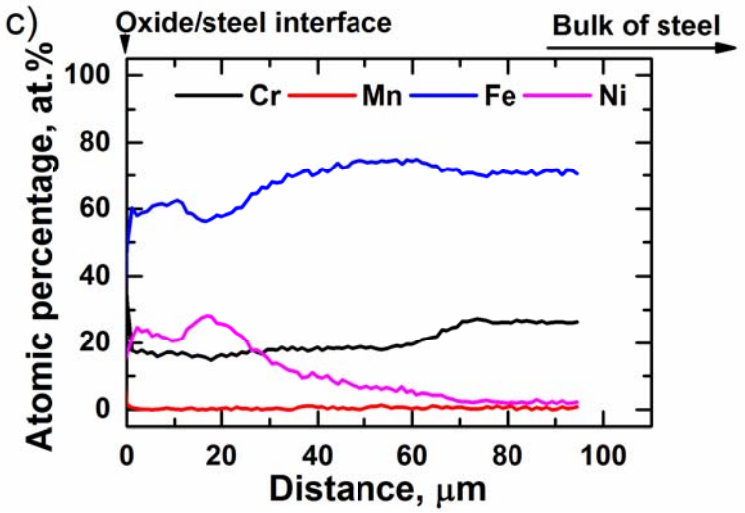

488

490 Figure 2. (a) Backscatter electron image and (b) EDS elemental map on the polished

491 cross-section of the oxide scale – steel (Crofer 22 APU) interface; (c) Integrated EDS

line-scan perpendicular to the oxide scale – steel (Crofer 22 APU) interface. The sample is a 300 μm thick Crofer 22 APU sheet coated with 13 μm thick Ni coating on both sides, further heat treated at 800 ^{o}C in H_2+N_2+H_2O for 2000 h.

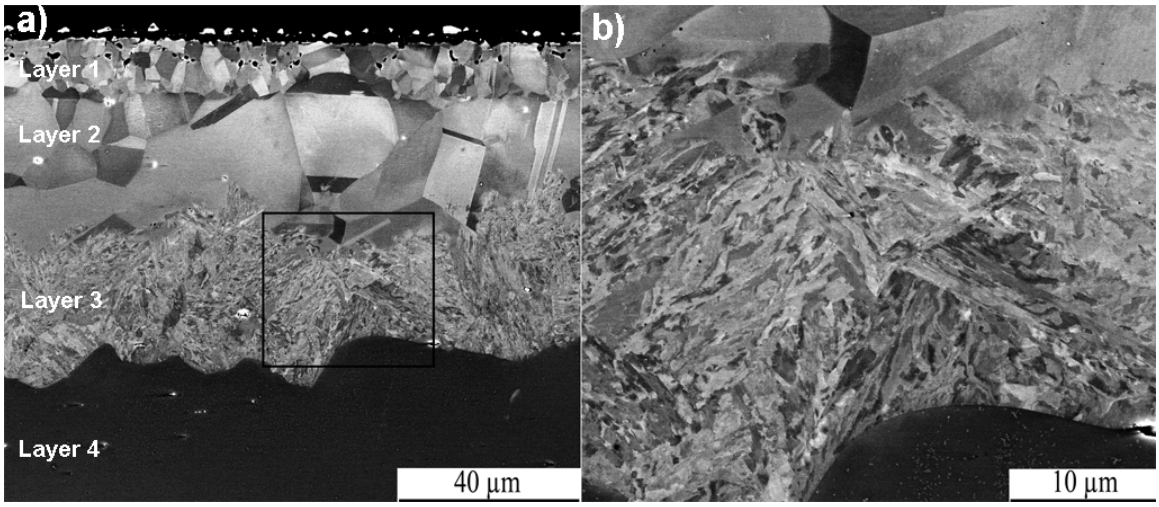

Figure 3. (a) Backscatter electron image covering all four distinct layers in the steel. (b) A higher magnification backscatter electron image of the region marked by the black square in (a) showing the fine-grained microstructure of Layer 3.

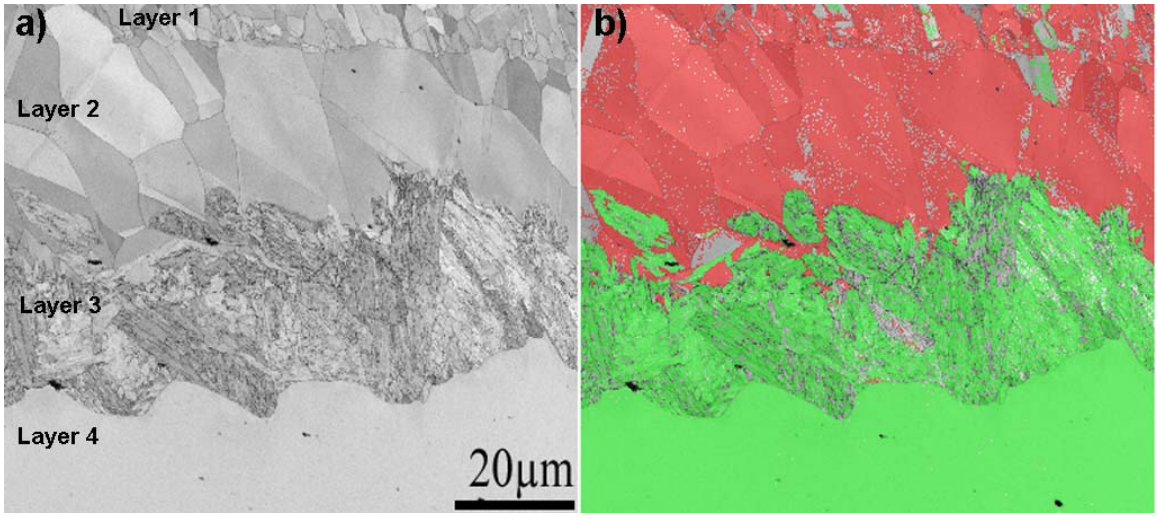

Figure 4. (a) Electron backscatter pattern quality (EBSP-Q) map of an area covering all four layers. (b) Color coded phase map (ferrite: green and austenite: red) overplayed on EBSP-Q map.

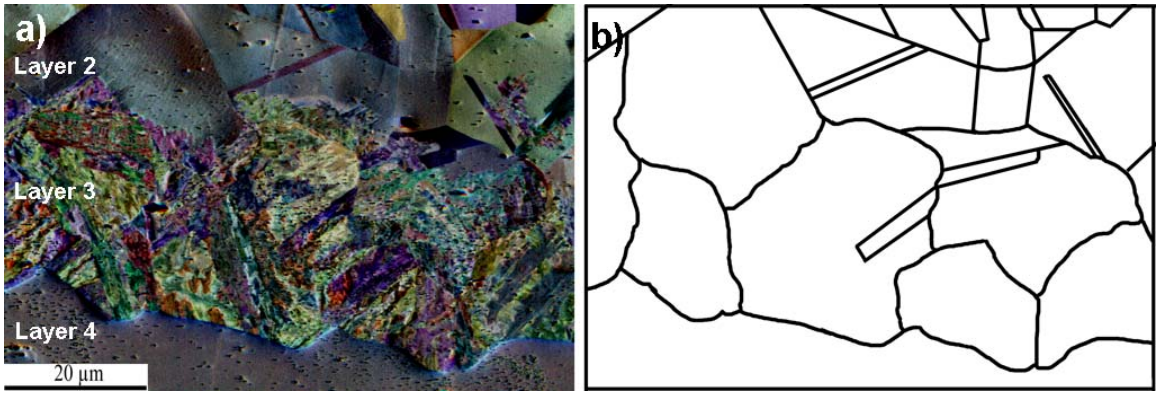

505

506 Figure 5. (a) ARGUS^{TM} image [15] of the Layers 2, 3 and 4. (b) A subjective

507 reconstruction of pre-austenite grains of Layer 2 and Layer 3.

508

509

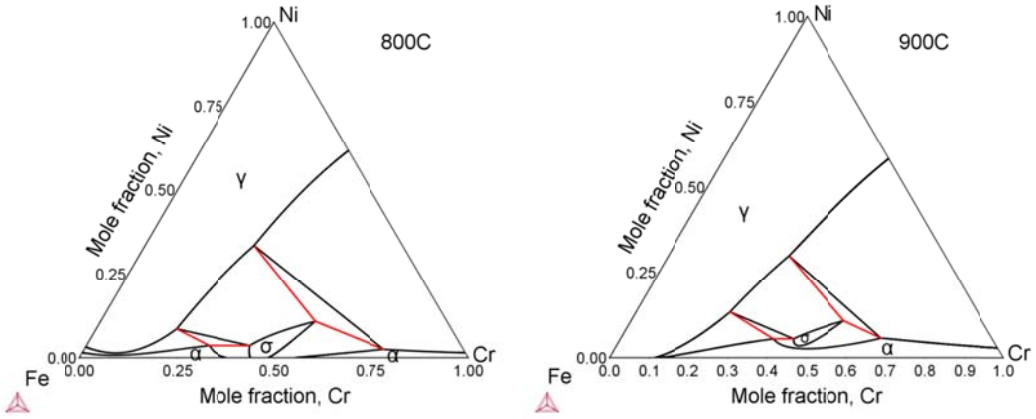

Figure 6. Phase diagrams of Fe-Cr-Ni at 800 and 900 ^{o}C. In the diagrams all the single-phase regions have been marked: α - BCC (ferrite), γ - FCC (austenite), and σ. The red triangles indicate 3-phase equilibrium (α+γ+σ), while the remaining unmarked regions are 2-phase equilibria (α+γ, γ+σ, or α+σ).

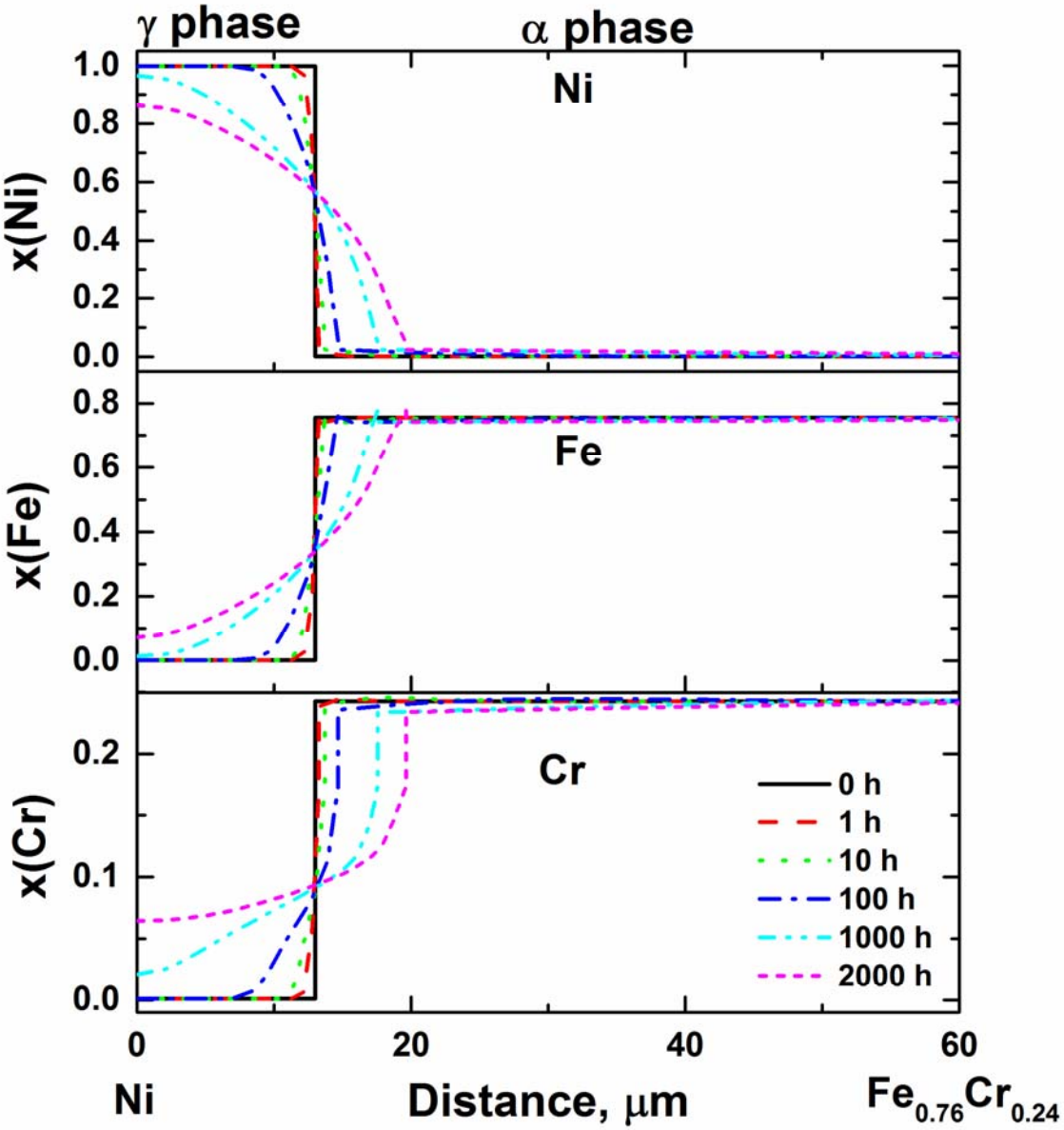

517

518 Figure 7. Calculated composition profiles (in mole fraction) along the diffusion couple of

519 Ni – $Fe_{0.76}Cr_{0.24}$ heat treated at 800 ^{o}C for periods up to 2000 h. The initial thickness was

520 13 μm and 150 μm for the Ni and $Fe_{0.76}Cr_{0.24}$ layers, respectively. Only bulk diffusion

521 was considered here.

522

523

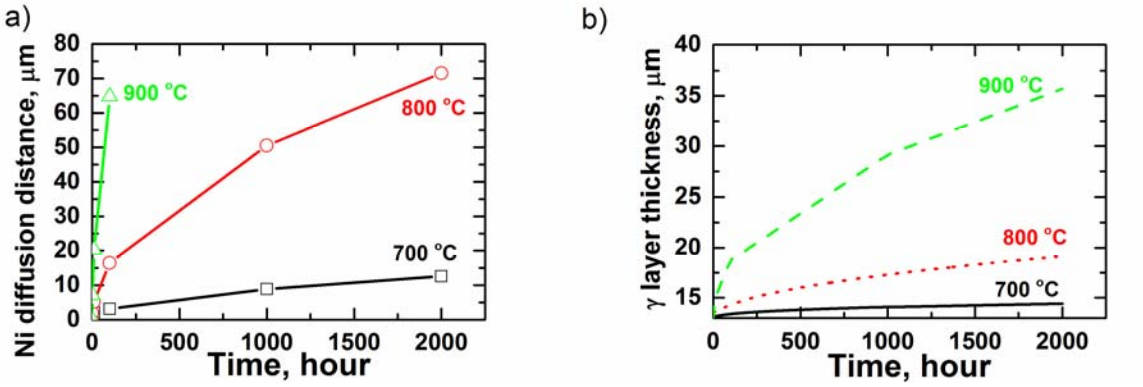

524

525 Figure 8. (a) Calculated Ni diffusion distance and (b) thickness of the γ layer in the
526 diffusion couple of Ni – $Fe_{0.76}Cr_{0.24}$ heat treated at 700-900 ^{o}C for periods up to 2000 h.
527 The initial thickness was 13 μm and 150 μm for the Ni and $Fe_{0.76}Cr_{0.24}$ layers,
528 respectively. The Ni diffusion distance is defined as the distance from the initial γ/α
529 interface at 0 h (i.e. Distance = 13 μm in Figure 1) to the position where the Ni content
530 reaches below 0.5 wt.%. Only bulk diffusion was considered here.

531

532

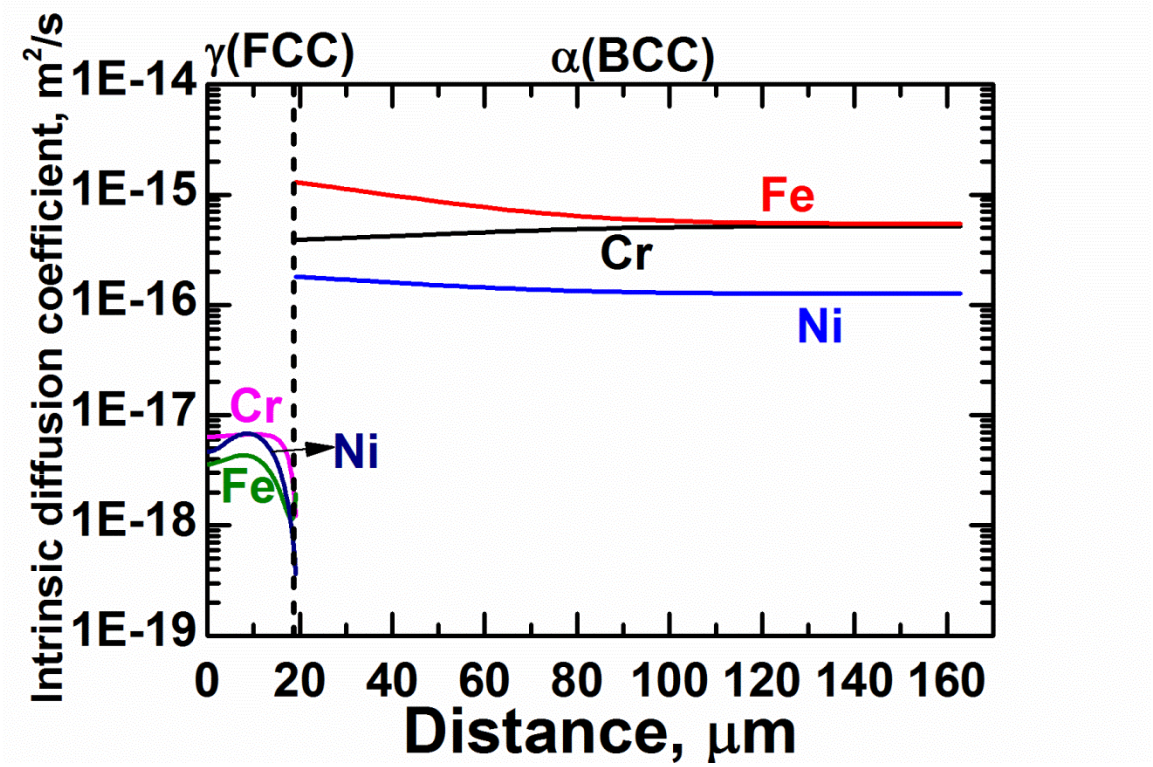

533

534 Figure 9. Intrinsic diffusion coefficients of Cr, Ni and Fe in α and γ phases along the

535 diffusion couple of Ni – $Fe_{0.76}Cr_{0.24}$ heat treated at 800 ^{o}C at *Time* = 2000 h. Only bulk

536 diffusion was considered here.

537

538

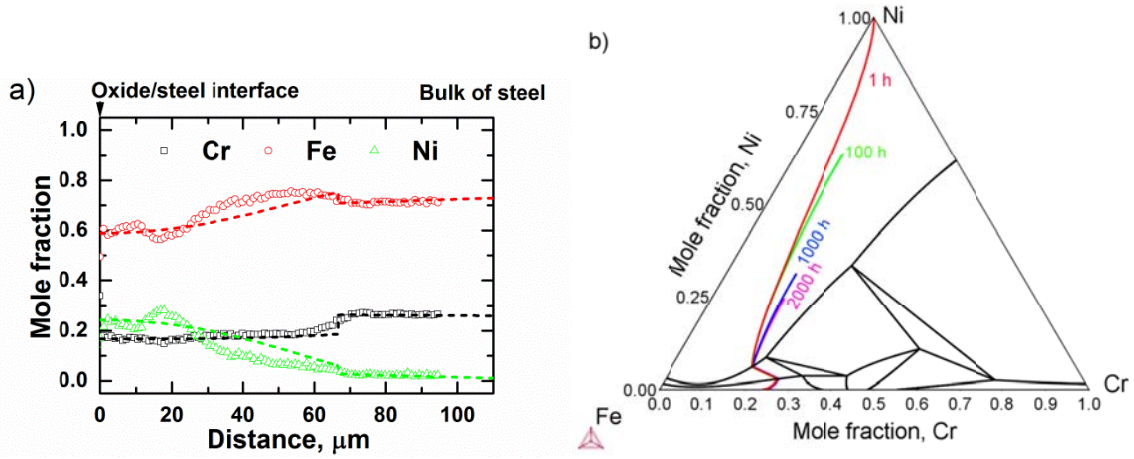

Figure 10. (a) Left: Simulated composition profiles (in mole fraction) along the diffusion couple of Ni – $Fe_{0.76}Cr_{0.24}$ heat treated at 800 ^{o}C for periods up to 2000 h. The initial thickness was 13 μm and 150 μm for the Ni and $Fe_{0.76}Cr_{0.24}$ layers, respectively. Both bulk and grain boundary diffusion are considered. The experimental data points are from the present work (Figure 2c). Mn was excluded in calculating mole fraction; (b) Right: diffusion path at 1 h (red), 100 h (green), 1000 h (blue), 2000 h (pink) super-imposed onto the Fe-Cr-Ni phase diagram at 800 ^{o}C.

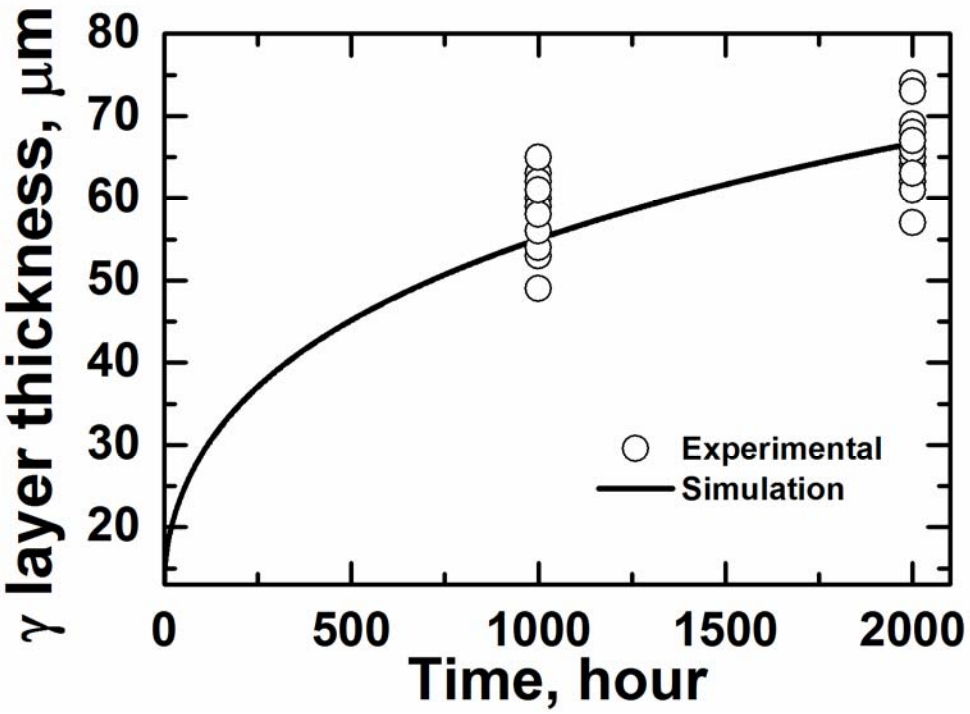

549

550 Figure 11. Thickness of the γ layer in the diffusion couple of Ni – $Fe_{0.76}Cr_{0.24}$ heat treated
551 at 800 ^{o}C for periods up to 2000 h. The initial thickness was 13 μm and 150 μm for the
552 Ni and $Fe_{0.76}Cr_{0.24}$ layers, respectively. The experimental values were obtained from SEM
553 image analysis, where the thickness of Layers 1+2+3 was measured at 20-30 different
554 locations.

555

556

557

558